Independent Positioning of Magnetic Nanomotors

Pranay Mandal,*,† Vaishali Chopra,† and Ambarish Ghosh*,†,‡,§

†Centre for Nano Science and Engineering, Indian Institute of Science, Bangalore 560012, India, ‡Department of Physics, Indian Institute of Science, Bangalore 560012, India, and §Department of Electrical Communication Engineering, Indian Institute of Science, Bangalore 560012, India

ABSTRACT There is considerable interest in powering and maneuvering nanostructures remotely in fluidic media using noninvasive fuel-free methods, for which small homogeneous magnetic fields are ideally suited. Current strategies include helical propulsion of chiral nanostructures, cilia-like motion of flexible filaments, and surface assisted translation of asymmetric colloidal doublets and magnetic nanorods, in all of which the individual structures are moved in a particular direction that is completely tied to the characteristics of the driving fields. As we show in this paper, when we use appropriate magnetic field configurations and actuation time scales, it is possible to maneuver geometrically identical nanostructures in different directions, and subsequently position them at arbitrary locations with respect to each other. The method reported here requires proximity of the nanomotors to a solid surface, and could be useful in applications that require remote and independent control over individual components in microfluidic environments.

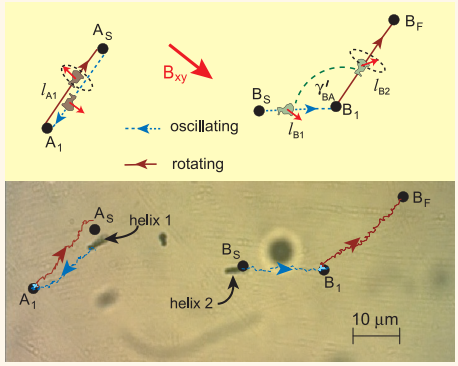

KEYWORDS: nanopropulsion · magnetic actuation · glancing angle deposition · active matter · independent control · nanomotors

Precise, fuel-free and remote manipulation[1−4] of nanoscale objects in fluidic media, including biological tissues and organs, can revolutionize[5] various aspects of nanomedicine,[6−9] such as microsurgery, *in vivo* sensing and drug delivery.[10] The most popular method of micromanipulation in fluidic environments is to use an optical tweezer,[11,12] which allows multiple objects to be maneuvered and positioned independently. In spite of the tremendous success of the optical tweezer in aiding various biological[13] measurements, the technique requires intense laser beams and close proximity to a focusing lens, and therefore not useful for remote operations in living systems. Furthermore, the manipulation technique only works well for dielectric objects larger than few hundred nanometers, although there are current efforts toward trapping metallic[14] particles of smaller dimensions. Some of these limitations do not exist when magnetic fields are used to maneuver small objects, since most living systems are compatible with strong magnetic fields, and the method works naturally with metals. Similar to optical tweezers, conventional magnetic manipulation[15] mostly relies on gradient[16] forces, as a result of which para- and ferromagnetic objects move toward the poles of a permanent magnet. The strength of the force scales with volume of the magnetic object and the gradient of the magnetic field, which renders the method useless[17] for remote manipulation of nanoscale objects.

The solution is to use time varying homogeneous magnetic fields with nanostructures of various symmetries, including flexible filaments,[18] helices[19−21] and colloidal doublets.[22,23] For example, rotating magnetic fields are commonly used to rotate ferromagnetic helical nanostructures about their long axes, which due to their inherent chirality translate, similar to various flagellated bacteria.[24,25] In the proximity of a surface, even achiral structures such as magnetic nanorods[26] and colloidal doublets can be rotated and thereby translated, owing to the time varying surface induced drag experienced by the rotating object. This strategy of inducing translational motion by time varying homogeneous magnetic fields have been used by many groups to design and develop various nanostructures, and study their motion in a wide variety of media including biologically important fluids,[27−31] such as undiluted

* Address correspondence to pranaymandal13@gmail.com, ambarish@ece.iisc.ernet.in.

Received for review September 29, 2014 and accepted March 30, 2015.

Published online March 31, 2015
10.1021/acsnano.5b01518

human blood.[32] Irrespective of the geometric details of the structure or the temporal profile of the applied field, a key feature remains common among all these strategies, in which the direction of the manipulated object is uniquely defined by the profile of the applied fields, which remains the same for a collection of nanostructures. Consider for example the motion of a helix in a rotating magnetic field. Irrespective of the details of the geometry or the material composition, helices always move in a direction perpendicular to the sense of rotation of the fields. Different degrees of freedom like the geometrical[33] features (*e.g.*, pitch and handedness of the helix) and the material composition may provide additional handles in controlling their speed,[34] but these methods do not allow independent direction and position control of the individual nanostructures.

RESULTS AND DISCUSSION

The strategy proposed (and demonstrated) here is to use the magnetic moment as the degree of freedom differentiating the direction of motion between the various nanostructures, shown schematically in Figure 1. Consider two nanoscale objects of identical shape and size, but with different directions of the magnetic moment in the body frame of reference. Under the action of a constant dc magnetic field, the structures get aligned, but do not move. The main challenge is to provide a source of energy to the structures that can be converted to directional motion, without losing the orientation imposed by the external dc field. This is similar in principle to many self-propelled[35] systems that can be driven externally, such as magnetotactic bacteria, where the source of kinetic energy is internal, but the alignment of the bacteria and therefore the direction of motion is entirely governed by the external magnetic (or even gravitational[36]) field. In the system reported here, we used oscillating magnetic fields to induce a rocking and thereby translational motion in the nanostructures due to their asymmetric shape. In addition to having different directions, one can aim toward "independent positioning" of the structures as well, for which it is necessary to add an actuation step in sequence such as to move them in an identical manner (illustrated in Figure 1). As we show here, both direction control and positioning can be achieved independently in a system of asymmetric helical nanostructures with efficient temporal design of homogeneous magnetic fields.

We used glancing angle deposition (GLAD[37]) to fabricate silica nanohelices above colloidal beads (polystyrene) and subsequently coated the objects with a magnetic material (*e.g.*, Cobalt). The direction of the permanent magnetic moment could be arbitrary with respect to the body frame of the helix, (see Methods section), or designed to be along a particular direction (see Supporting Information). The helices

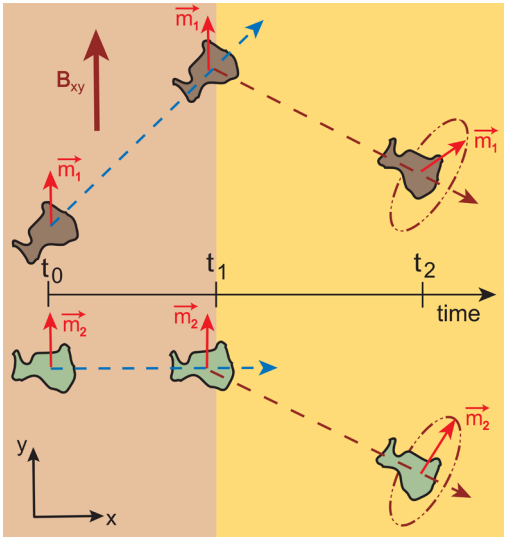

Figure 1. Schematic representation of the method used to position a pair of nanostructures at arbitrary locations with respect to each other. Two nanostructures of identical geometrical characteristics have different directions of permanent magnetization with respect to their body axis. Under the influence of a source of kinetic energy (here, externally applied oscillating magnetic fields), the objects move in different directions, while maintaining their alignment to the external applied dc field (B_{xy}). In the system described in this manuscript, the translational motion under oscillating fields originates in the asymmetric drag acting on the structures close to the bottom wall of the microfluidic chamber. At time t_1, the magnetic field configuration was changed (here, to rotating fields) such as to move them in an identical fashion, here screw-like motion. As a result, the final positions of the structures at time t_2 can be made completely arbitrary with appropriate choices of the applied field characteristics and times t_1, t_2.

(total length ~5 μm) were dispersed in deionized water in a microfluidic device of thickness around 30 μm, where they settled close to the bottom surface. The device was placed inside a triaxial Helmholtz coil built around an inverted optical microscope. Three current amplifiers were used to apply homogeneous magnetic fields with independent amplitudes, frequencies and phases in the three directions. Under the action of a dc magnetic field (B_{xy} = 2.8 G) along *y*-direction, which was also the image plane of the optical setup, the magnetic moments of the helices aligned with the field, as shown in Figure 2A (optical images in the inset). To provide kinetic energy to the structures, we added an oscillating field along the *z*-direction that was perpendicular to the plane (*x*−*y*) containing the helices. This resulted in the net field vector (**B**) tracing out an arc in the *y*−*z* plane (see Figure 2B), of arc angle less than 180°. The resultant dynamics of the helices, under the action of the dc and the oscillating fields, is shown in Figure 2C using schematic and experimental images. At the oscillation field amplitude of 60 G and frequency 40 Hz, respectively, the helices executed rocking motion in a plane perpendicular to the bottom surface (see Supporting Information Movie SM1), while turning about their own axis as well. The rocking

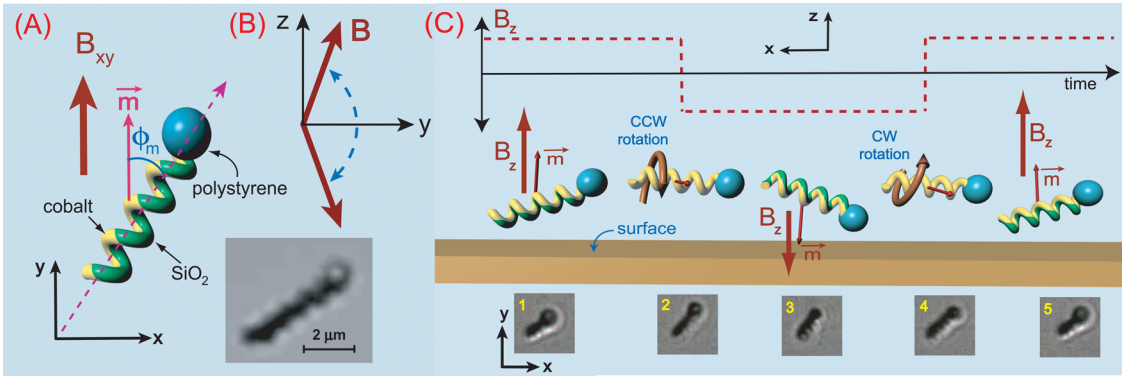

Figure 2. (A) Schematic of a nanohelix with magnetic moment aligned along the direction of an applied dc field. Inset shows a typical optical microscopy image. (B) Combined action of an oscillating field (B_z) along *z* direction and a dc field (B_{xy}) along *y*-direction in the *x*−*y* plane, such that the field vector (B) traces out an arc in the *y*−*z* plane. (C) Schematic of the rocking motion of the object under the combined action of the fields (B_z and B_{xy}). The optical images (taken from movie SM1) show a small modulation in the projected length of the object in the *x*−*y* plane, as would be expected for rocking motion in *x*−*z* plane. The orientation of the helices, same as their direction of motion, showed a small periodic variation around a constant mean direction.

motion of the helix was due to the fact that its magnetic moment got aligned in direction of the oscillating field while the sense of rotation (clockwise or counter clockwise) was determined by the direction of B_{xy} in *x*−*y* plane. The rocking motion was reflected in a slight modulation of length in the microscopy images (for clearer visualization, see Supporting Information Movie SM1). Most crucially, the orientation of the helices in the *x*−*y* plane remained almost constant, with some periodic variation superimposed. This can be seen clearly in the microscopy images in Figure 2C, where the helices under the combined action of B_z and B_{xy} were oriented in almost the same direction as the helices under the dc field alone (shown in the inset of Figure 2A). This shows clearly that the directionality of the helices remained in spite of the input of external energy into the system through fast oscillating magnetic fields.

To obtain a quantitative understanding of the orientation of the nanohelix under the combined action of oscillating (B_z) and dc (B_{xy}) magnetic fields, we used a numerical model that have been described in some of our earlier publications,[38,39] and has been described in the Methods section. The structure was approximated to be of ellipsoidal shape with effectively two rotational and two translational drag coefficients. We assumed the values corresponding to bulk liquid. To quantify the orientation, as shown in the inset of Figure 3, we have defined α as the angle made by the x-y projection of the rotating object to the dc field (*y*-axis). We assumed the applied dc field to be along the *y*-axis, and the initial position of the ellipsoid in the *x*−*y* plane oriented at an angle $\alpha = 5°$. The rotational dynamics of the ellipsoid was obtained from the angular velocities ($\boldsymbol{\omega}$) which were proportional to the net magnetic torque (**T**) acting on the objects through the relation $\mathbf{T} = \gamma\boldsymbol{\omega}$, where γ is the friction coefficient tensor. The calculations predicted precessional motion similar to what was observed in the experiments (see Supporting Information Movie SM1) and the schematic images shown in Figure 2. Of particular interest was the temporal variation of α, which has been shown in Figure 3A, for three different values of ϕ_m and two values of the magnetic moment. The steady state orientation could be represented by a periodic variation $\delta\alpha$ at the frequency of the oscillating field, superimposed over a mean direction $\langle\alpha\rangle$. In the absence of an oscillating field, the orientation of the ellipsoid corresponded to their magnetic moment aligned along B_{xy}, implying $\langle\alpha\rangle = \phi_m$, with $\delta\alpha = 0$. Interestingly, even in the presence of the oscillating field, for the parameters used in our simulations and experiments, the value of $\langle\alpha\rangle$ remains close (but not the same) to ϕ_m, implying the object to remain oriented along a similar direction. Consider for example the results shown in Figure 3, where the graphs depicted in black, red and blue correspond to ellipsoids of same magnetic moment but different ϕ_m. The dynamics of the ellipsoid with $\phi_m = 30°$ (shown in blue) showed mean steady state orientation of $\langle\alpha\rangle = 30°$ with higher $\delta\alpha$ (~2.5°), while the mean orientation changed to $\langle\alpha\rangle = 45°$ for $\phi_m = 60°$ (shown in black), with a smaller $\delta\alpha$ (~1.5°).

Note that the dynamics and therefore the value of $<\alpha>$ and $\delta\alpha$ can depend on many different parameters, such as the field strength, frequency, as well as the magnitude and direction of the permanent magnetization. This can be clearly seen in the graphs in blue and green in Figure 3A, which correspond to same $\phi_m = 30°$, but two different magnetization values 1.7×10^{-15} and 3.4×10^{-15} Am^2, respectively. The dynamics of the ellipsoid with larger magnetic moment (shown in green) settled to a different $\langle\alpha\rangle$ (~18°) and a larger $\delta\alpha$ (~3°), compared to the ellipsoid with smaller magnetic moment (shown in blue). The most important point to note is that ellipsoids with different ϕ_m indeed oriented in different directions under identical magnetic field configurations, which is the central requirement in obtaining independent directionalities.

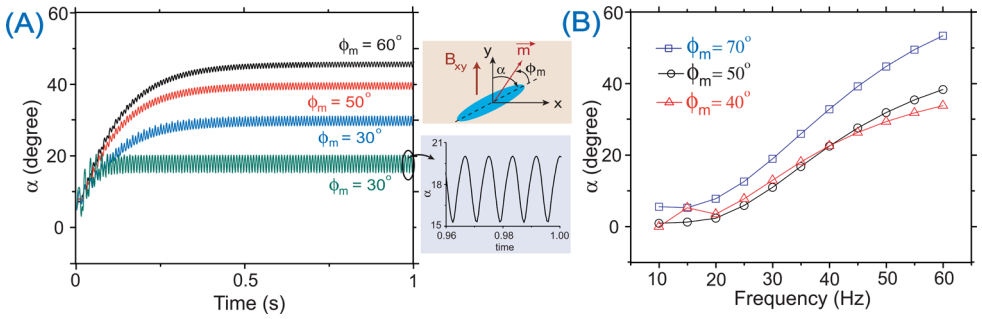

Figure 3. (A) Calculation of the orientation (α) as a function of time, under the combined action of B_z and B_{xy}. The upper inset shows the convention used at any given instant of time. We assumed objects with different directions of magnetization, quantified by ϕ_m, the angle between the direction of magnetization and the long axis of the ellipsoid. The initial orientation was assumed to be at 5° to the *y*-axis for all the simulations. The black, red, and blue curves correspond to structures with magnetic moment value 1.7×10^{-15} Am^2 and $\phi_m = 60°$, 50°, and 30°, respectively, while the green curve corresponds to magnetic moment value 3.4×10^{-15} Am^2 and $\phi_m = 30°$. The lower inset shows a periodic variation of the orientation at the frequency of B_z, whose amplitude depends on the direction of magnetization, as well as strength of the magnetic moment and magnetic fields. (B) The dependence of the steady state orientation on frequency of the oscillating magnetic field for different values of ϕ_m.

Crucially, the final orientation depended on the frequency of the oscillating field as well as ϕ_m, as shown in Figure 3B, implying the relative orientation of the objects can be tuned by choosing appropriate magnetic field frequency. Effects of thermal fluctuations were not taken into consideration in these calculations, which may be important at low magnetic field frequencies[40] when the actuation time scales are comparable to the rotational diffusion times of the ellipsoid about its long axis.

While the numerical calculations provide insight into how the objects retain different directionalities while performing rocking motion under the action of B_{xy} and B_z, the question that raises itself is how the rocking motion resulted in a net translation, such as the trajectory shown in Figure 4A. Due to fixed dc field (B_{xy}), the direction of the torque experienced by the nanohelix along its long axis changes alternately at each turning events (see Figure 2C). As a result, the nanohelix performed alternate clockwise and counterclockwise rotations which resulted in back-and-forth (reciprocal) motion. This is shown in the inset of Figure 4A. There are a couple of ways[41] in which reciprocal[42] movements can lead to net translation at low Reynolds numbers, of which most relevant in the present system, was the proximity of the object to the bottom surface of the fluidic chamber. The origin of net translation out of the reciprocal movements was related to the inherent structural asymmetry of the nanohelices, which was primarily due to the difference in the drag faced by the helix as its two ends approached the chamber surface. This was similar to the way translation was induced in rotating magnetic nanorods[26] and colloidal doublets,[22] and explains how the rocking motion led to back and forth translation. The difference in the drag force was due to the presence of the colloidal bead at one end of the helix; the drag experienced by the object depended on whether the configuration corresponded to either tail (without bead, panel 1 of Figure 2C) or head (with bead, panel 3 of Figure 2C) of the structure in closest proximity to the bottom surface. A detailed numerical model to quantify the net translation arising out of the differential[43] surface drag between the two configurations is beyond the scope of this manuscript. This is primarily because the calculations depend sensitively on the distance of the objects from the chamber surface, which could not be determined experimentally. A control experiment, however, provided valuable insight in support of this argument. We modified the nanohelix to remove the colloidal bead (details in Methods section), thus corresponding to a geometry that was significantly more symmetric at the ends. As shown in the inset of Figure 4A (shown in red), the net translation speed of the symmetric structure (~1 μm/s) was measured to be almost 6 times smaller compared to the asymmetric object (~5.5 μm/s), thereby validating the mechanism proposed here. The speed of the nanohelices depended on the frequency and ϕ_m in a nontrivial way, as shown in Figure 4B. For a particular ϕ_m, the speed increased linearly with the frequency of the oscillating field, but then reduced beyond a critical frequency. The critical frequency depended on the strength of the magnetic field, which is probably related to the applied magnetic torque (depends on field strength) being balanced by the viscous drag (depends on the frequency). As shown, the critical frequency for 15 G was 15 Hz, while for 30 G it was about 25 Hz, and the slope of the speed-frequency graph remained constant for a particular angle of magnetization for frequencies lower than critical. We found an increase in the slope of the speed-frequency curve when the angle of magnetization was decreased from 66° to 59°. The direction of the translational motion, as shown in Figure 4C, could be controlled by changing the direction of the dc fields, with very high precision. Two of these trajectories were obtained from Movies SM2 and SM3, available in the Supporting

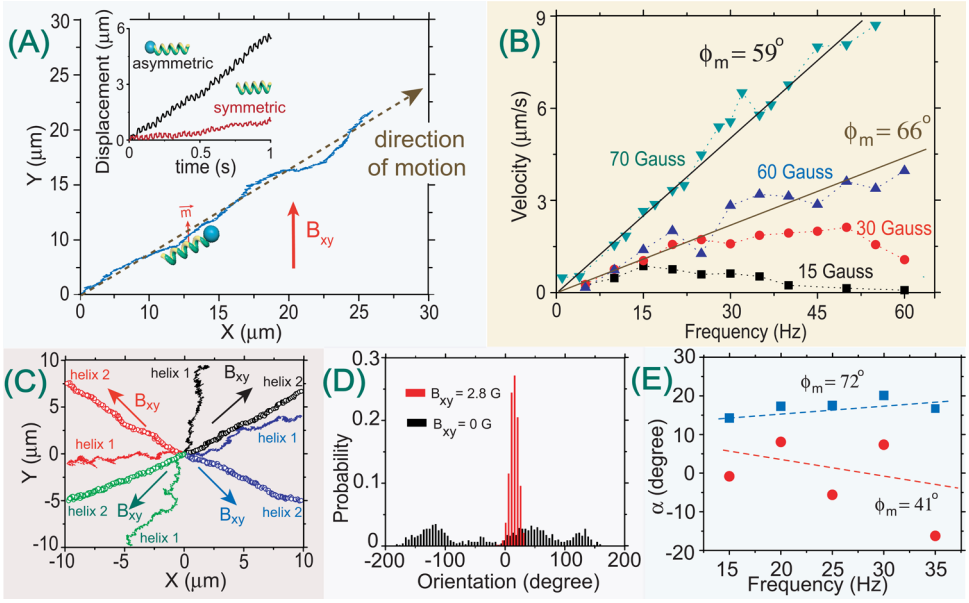

Figure 4. (A) Trajectory of a nanohelix in the $x-y$ plane under oscillating (along z) and dc fields (along y). The alignment of the object and therefore the direction of motion were determined by the direction of the applied dc field. (Inset) The back and forth motion of the object at the frequency of the oscillating field, resulting in a net displacement over time. The two curves correspond to an asymmetric (with head, black) and a symmetric (without head, red) helix under almost identical experimental conditions. (B) Measured speed of the nanohelices as a function of frequency of the oscillating field. The black, red, and blue data points correspond to a helix of $\phi_m = 66°$ for different field strengths (15, 30, and 60 G), while the green data points were for a helix of $\phi_m = 59°$. (C) Controlling the direction of motion by changing the direction of the dc field (arrows of different colors, strength = 2.8 G) for two nanohelices with different directions of magnetization ($\phi_m = 35°$ and 43° for open helix 1 and helix 2, respectively). Trajectories corresponding to four directions of the applied dc fields are shown. (D) Probability distribution of the orientation of a helix with and without the dc fields. The lack of directional motion when the dc field was reduced to zero can be clearly seen. (E) Measured dependence of the steady state orientation of two nanohelices with different ϕ_m on frequency of the magnetic field.

Information, which differed in the direction of the applied dc field. We performed experiments with two nanohelices of different ϕ_m and different directions of dc magnetic field, and found the relative angle between the nanohelices at a particular frequency remained constant irrespective of the direction of the dc field. The motion of the helix became nondirectional when the dc field in the $x-y$ plane was reduced to zero, even though the oscillating field in the z-direction remained. In this case, the helices did not move in a particular direction, but instead showed reciprocal back and forth movements with enhanced diffusivity.[44] The randomized orientation of the helices in the absence of the dc field can be seen in Figure 4D. As a final characterization, we measured the orientation of two nanohelices of different ϕ_m as a function of frequency. While the orientation of one of the helices changed slightly as a function of frequency ($\phi_m = 72°$), the direction of the object with a different $\phi_m = 41°$ had more variation with frequency. We are not sure why the experimental data with the helix of $\phi_m = 41°$ was significantly noisier than the other helix; however, that the orientation of a nanohelix depended on frequency, was in agreement with the numerical calculations shown in Figure 3B.

The working principle of the system presented here is very similar to that of magnetotactic bacteria, which are living self-propelled objects but whose directionality can be controlled by dc magnetic fields. The additional handle available in the present system was the direction of the magnetic moment, which could be along arbitrary directions and therefore could allow individual direction and position control as postulated in the discussion of Figure 1. The details are shown in Figure 5A, where the nanostructure A is maneuvered with oscillating fields and then brought back to its original position with appropriately chosen configuration of rotating magnetic fields. The nanostructure B, with a different ϕ_m moves in a direction at angle γ'_{BA} to the direction of A during the step with the oscillating field, but moves parallel during the step with the rotating field. This results in a net displacement of B which can be made completely arbitrary by choosing the duration of the actuation steps and the direction of the dc field. A detailed mathematical proof on the same is provided in the Supporting Information.

An experimental demonstration of this idea is shown in Figure 5B (also see Supporting Information Movie SM4). Two helices with different directions of magnetization were actuated with an oscillating field of 50 G at 30 Hz, over which a dc magnetic field of 1.5 G in the $x-y$ plane was superposed. The trajectories marked in blue were taken over 3.2 s, and found to be in separate directions with an angular separation of ~130° that

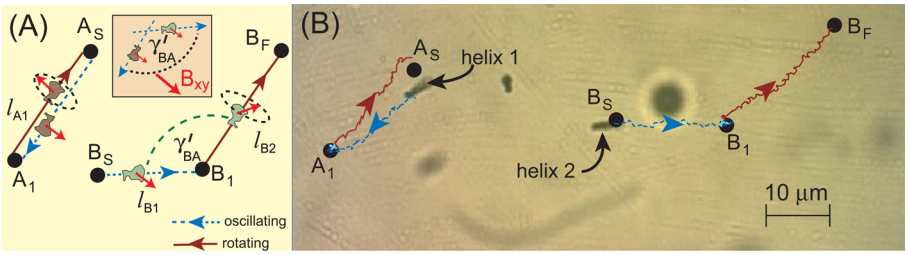

Figure 5. Independent positioning of two nanohelices. (A) Schematics for actuation principle of independent positioning. Initial positions of the two nanostructures (violet and green) with different ϕ_m are A_S and B_S, respectively. The two nanostructures are first actuated by oscillating field of frequency (f_o) with dc field (B_{xy}) along a particular direction, as shown in the inset. The oscillating field was applied for t_o seconds such that first nanostructure (violet) moves to A_1, while the other (green) moves to B_1. Finally, a rotating field is applied for t_R seconds to bring back the first structure (violet) to its original position and simultaneously position the other (green) at a desired position at B_F. (B) Experimental demonstration of independent positioning, where oscillating and dc fields were used for 3.2 s, to move the helices in different directions, as determined by their directions of magnetization and f_o. The fields were then turned off for 1.6 s, after which a rotating field was used for 6.7 s to move the objects in parallel paths. The trajectories were obtained from the movie SM4.

was roughly the same as the difference in their magnetization angles. To position the nanohelices with complete independence, a second step was necessary, where the two helices were actuated in an identical fashion. This was achieved by applying rotating magnetic fields of strength 30 G and 25 Hz. The choice of the frequency was such that the helices, in spite of the differences in the magnetization vectors, show corkscrew motion[38,39,45] in a direction perpendicular to the plane of the rotating field. Trajectories marked with red show the parallel paths taken by the objects, thereby reaching a final configuration that was completely independent of the initial positions. For the particular case reported here, one of the helices was brought back close to its original position, while the other helix was displaced by almost 40 μm in an arbitrary (but desired) direction.

A question that naturally arises is whether this strategy can be extended to more than two particles. We consider three particles A, B, and C, and aim to find a combination of magnetic actuation steps that will allow C to be moved at a certain location, while A and B return to their original positions. Building upon the methodology followed for two particles, as shown in Figure 5A, we use an oscillation and a rotating field step to take from $\mathbf{A_S}$ to $\mathbf{A_1}$, and then back to $\mathbf{A_S}$. The directions of motion of B and C are tied to the direction taken by A, given by γ'_{BA} and γ'_{CA}, respectively. Accordingly, the paths taken by B and C are given by $\mathbf{B_S} - \mathbf{B_1} - \mathbf{B_2}$ and $\mathbf{C_S} - \mathbf{C_1} - \mathbf{C_2}$, respectively. The next step would be to take A and B to its original position $\mathbf{A_S}$ and $\mathbf{B_S}$, respectively, while C goes to a location different from its original. Consider the possibility shown in Figure 6A, where we have assumed one more step of oscillating and rotating field. The paths taken by A and B to return to their original positions are given by $\mathbf{A_S} - \mathbf{A_2} - \mathbf{A_S}$ and $\mathbf{B_2} - \mathbf{B_3} - \mathbf{A_S}$, respectively. If the oscillating steps are taken at the same frequency, the directions of B and C with respect to A (and each other) are fixed, given by γ'_{BA} and γ'_{CA}, respectively. This is a crucial point, since this implies the path taken by B would have to be a parallelogram with two parallel steps from the rotating field and two equal angles (γ'_{BA}) enclosed. This would automatically imply a similar fate for C, resulting in its return to its original position (see Supporting Information for detailed mathematical proof). The strategy to maneuver three particles independently would therefore be possible if the second oscillating step is taken at a different frequency, such that the directions taken by B and C with respect to A (given by γ''_{BA}, γ''_{CA}) are different from γ'_{BA}, γ'_{CA}. This is shown in Figure 6B, where the path taken by B to return to its starting position is not a parallelogram, and the final position of C is different from its original location.

To make this analysis very general, it is easy to see how the various steps can be combined leaving only steps that are at distinct angular relations with respect to each other. This is shown in Figure 6C, where the closed paths $\mathbf{A_S} - \mathbf{A_1} - \mathbf{A''_2} - \mathbf{A_S}$ and $\mathbf{B_S} - \mathbf{B_1} - \mathbf{B''_3} - \mathbf{B_S}$ are obtained by one rotating and two oscillating steps at different frequencies, which at the same time results in a distinct displacement of C. To extend this to n helices, one would have to combine n steps that are of different angular relationship with respect to each other, such as $n - 1$steps of oscillating fields at different frequencies and one step of rotating field.

CONCLUSION

Commonly used methods of magnetic manipulation, such as those based on field gradients, have a fundamental limitation in which the direction of motion remains the same across all the objects. There have been several attempts to overcome this limitation, using strategies based on magnetic composition[46] and geometrical[47] characteristics, such as to move individual objects in different directions. These strategies are all based on magnetic gradient force that is ineffective at the nanoscale, which is the premise of this work. Magnetic nanopropulsion typically relies on rotating or undulating homogeneous

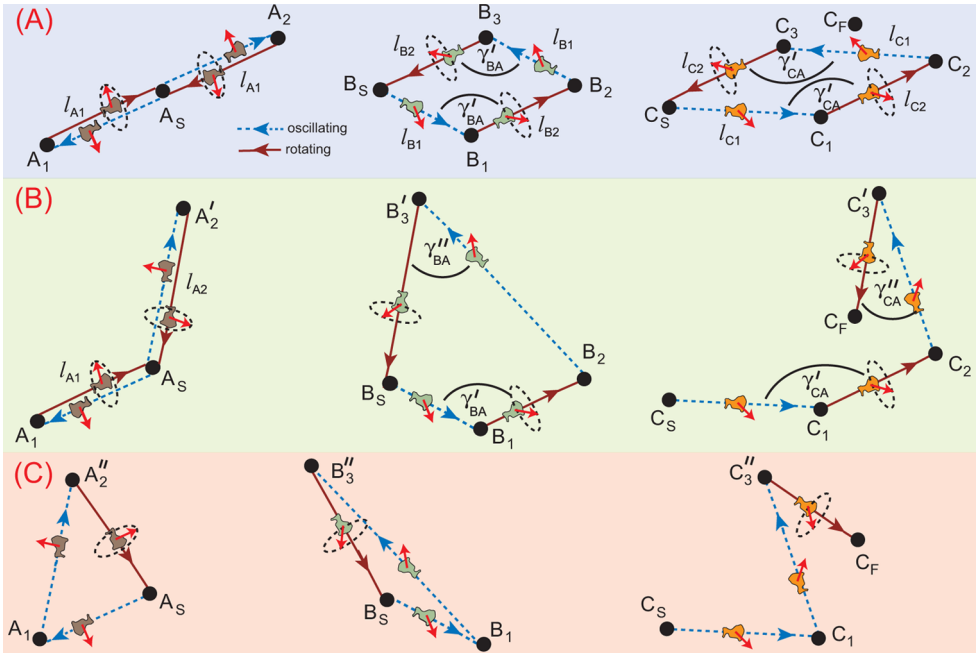

Figure 6. Independent positioning of more than two nanohelices. (A) Actuation with two oscillating steps at the same frequency (and therefore same γ'_{BA}, γ'_{CA}) followed by two steps with rotating fields will result in all three helices returning to their original positions. (B) Actuation with two oscillating steps at different frequencies (and therefore different γ'_{BA}, γ'_{CA}, γ''_{BA}, γ''_{CA}) followed by two steps with rotating fields can result two of the helices returning to their original positions, while one helix is displaced by a certain amount at a particular direction. (C) Simplification of the strategy shown in (B). Two oscillating steps at different frequencies followed by a single rotating step can also result in two helices with zero displacement and one helix moved to a predetermined position.

magnetic fields, used to actuate structures of various asymmetric geometries, such as helices, rods close to a surface, *etc*. These strategies suffer from the same limitation in which all the nanostructures move along the same direction, although there have been efforts to achieve independent control on their speeds. As we have demonstrated here, it is possible to actuate a pair of magnetic nanohelices in different directions and position them at arbitrary locations with respect to each other. The solution achieved in this paper was inspired from the working principle of magnetotactic bacteria[48,49] and catalytic nanomotors[50−52] containing magnetic elements, whose the source of power and the steering mechanism were effectively decoupled, by using magnetic fields that vary at significantly different time scales. In the present method, the source of power was derived from an oscillating magnetic field, while dc fields in the $x-y$ plane were used to steer the nanohelices. Although the present system was based on a combination of cork-screw and surface-assisted propulsion of helical nanostructures, the method is general enough to be applicable to other magnetic nanopropulsion systems as well. For example, one could incorporate ferromagnetic elements in various types of self-propelled systems, such as chemically powered catalytic nanomotors, light driven Janus particles, bubble driven nanotubes, *etc*. and magnetize them at different angles with respect to their body axes. These objects, in the presence of a dc magnetic field, would travel in different directions determined by their direction of magnetization, and travel in arbitrary directions in the absence of magnetic fields. The manipulation method reported here could be useful in microfluidic applications that require precise assembly of individual components. Finally, it will be interesting to investigate the role of fluidic interactions in a collection of nanostructures moving in coupled but different directions, which may lead to the emergence of novel collective phenomena.[53−55]

METHODS

Experimental Section. The method of fabrication and actuation of the ferromagnetic nanohelices over a well separated[56] monolayer of colloidal beads has been described in detail in earlier publications.[21,39,40] The nanohelices were laid down on a wafer, which was subsequently coated with a magnetic material. For the control experiment requiring symmetric structures, we treated the wafer with laid down nanohelices with Piranha solution to remove the head (colloidal bead) of the structure, before coating with the magnetic material. This caused the polystyrene bead to be etched away completely, while the rest of the structure, made of SiO_2, remained intact. The nanohelices coated with the magnetic material were magnetized in a direction parallel to the plane of the wafer, which resulted in permanent magnetization of the nanohelices that were in random directions with respect to their body axes.

Numerical Calculations. We simulated the orientation of an ellipsoid under magnetic actuation, as described in the main text. For representation of the orientation angles of the nanohelix in the numerical simulation, we have followed *x*-convention, where at any instant of time *t*, the orientation of the nanohelix was represented by unit quaternion $q_0(t)$, $q_1(t)$, $q_2(t)$ and $q_3(t)$. The magnetic moment ($\vec{m}$) of the nanostructure at an angle φ_m with respect to its long axis (as shown in the schematics of Figure 3) is represented by a vector form as $[m \times \sin(\varphi_m) \quad 0 \quad m \times \cos(\varphi_m)]$ in the body fixed coordinate frame, where '*m*' represents the strength of the magnetic moment. The applied magnetic field in lab fixed coordinate is given by $\vec{B}_{LF} = [0\ B_{xy}\ B_{square}]$, where B_{square} represents magnetic field along *z*-direction varying as a square wave with frequency *f*. After each time step (Δt), the applied magnetic field in body fixed frame (B_{BF}) was calculated by $B_{BF} = R \times B_{LF}$, where *R* is the rotational matrix represented by

$$R = \begin{bmatrix} q_0^2+q_1^2-q_2^2-q_3^2 & 2(q_1q_2+q_3q_0) & 2(q_1q_3-q_2q_0) \\ 2(q_1q_2-q_3q_0) & q_0^2-q_1^2+q_2^2-q_3^2 & 2(q_2q_3+q_1q_0) \\ 2(q_1q_3+q_2q_0) & 2(q_2q_3-q_1q_0) & q_0^2-q_1^2-q_2^2+q_3^2 \end{bmatrix}$$

The dynamical time evolution of the orientation of the nano helix was solved in the body fixed coordinate system, given by $\vec{m} \times \vec{B}_{LF} = \gamma\vec{\omega}$. In this expression, $\vec{\omega}$ represents the angular velocity of the ellipsoid in body fixed coordinate system and γ is rotational drag tensor given by

$$\begin{bmatrix} \gamma_s & 0 & 0 \\ 0 & \gamma_s & 0 \\ 0 & 0 & \gamma_l \end{bmatrix}$$

where γ_s and γ_l are the rotational drag of the ellipsoid along its short axis and long axis, respectively. After each time step Δt, quaternions were updated by $q(t + \Delta t) = q(t) + \dot{q}\Delta t$, such that the rate of change of quaternions is given by $\dot{q} = (1/2)W^T\vec{\omega}$ where

$$W = \begin{bmatrix} -q_1 & q_0 & q_3 & -q_2 \\ -q_2 & -q_3 & q_0 & q_1 \\ -q_3 & q_2 & -q_1 & q_0 \end{bmatrix}$$

Note that Δt considered in the simulation is $\sim 10^{-5}$ seconds, which is much smaller than any other time scale involved in the system. For an ellipsoid, the drag coefficients are given as $\gamma_s = (32\pi\mu(a^4 - b^4))/(3S(2a^2 - b^2) - 2a)$ and $\gamma_l = (32\pi\mu(a^2 - b^2)b^2)/(3(2a - b^2S)$ where $S = (2/(a^2 - b^2)^{1/2})\ \ln((a + (a^2 - b^2)^{1/2})/b)$, μ is the viscosity of water (9×10^{-4} Pa·s), a (= 2.5 μm) and b (= 0.5 μm) are the lengths of the semimajor and semiminor axes of the ellipsoid, respectively. With these parameters, we obtained $\gamma_s \sim 6 \times 10^{-20}$ kg·m^2/s and $\gamma_l \sim 10^{-20}$ kg·m^2/s.

Conflict of Interest: The authors declare no competing financial interest.

Acknowledgment. The usage of the facilities in Micro and Nano Characterization Facility (MNCF, CeNSE) at IISc, and funding from the Department of Biotechnology is gratefully acknowledged. This work is partially supported by the Ministry of Communication and Information Technology under a grant for the Centre of Excellence in Nanoelectronics, Phase II.

Supporting Information Available: Movies SM1–4, as discussed in the main text. SM1 is slowed down 15-fold for easier visualization. Also available is the methodology to obtain arbitrary ϕ_m in the nanohelices and the mathematical analysis of the various actuation strategies discussed in the main text. This material is available free of charge *via* the Internet at http://pubs.acs.org.

REFERENCES AND NOTES

1. Ozin, G. A.; Manners, I.; Fournier-Bidoz, S.; Arsenault, A. Dream Nanomachines. *Adv. Mater.* **2005**, *17*, 3011–3018.
2. Ebbens, S. J.; Howse, J. R. In Pursuit of Propulsion at the Nanoscale. *Soft Matter* **2010**, *6*, 726–738.
3. Fischer, P.; Ghosh, A. Magnetically Actuated Propulsion at Low Reynolds Numbers: Towards Nanoscale Control. *Nanoscale* **2011**, *3*, 557–563.
4. Mallouk, T. E.; Sen, A. Powering Nanorobots. *Sci. Am.* **2009**, *300*, 72–77.
5. Feynman, R. P. There's Plenty of Room at the Bottom. *Eng. Sci.* **1960**, *23*, 22–36.
6. Wang, J.*Nanomachines: Fundamentals and Applications*; Wiley-VCH: Weinheim, 2013.
7. Wang, J.; Gao, W. Nano/Microscale Motors: Biomedical Opportunities and Challenges. *ACS Nano* **2012**, *6*, 5745–5751.
8. Wang, J.; Manesh, K. M. Motion Control at the Nanoscale. *Small* **2010**, *6*, 338–345.
9. Martel, S.; Mathieu, J.-B.; Felfoul, O.; Chanu, A.; Aboussouan, E.; Tamaz, S.; Pouponneau, P.; Yahia, L. H.; Beaudoin, G.; Soulez, G.; Mankiewicz, M. Automatic Navigation of an Untethered Device in the Artery of a Living Animal Using a Conventional Clinical Magnetic Resonance Imaging System. *Appl. Phys. Lett.* **2007**, *90*, 114105–3.
10. Dogangil, G.; Ergeneman, O.; Abbott, J. J.; Pane, S.; Hall, H.; Muntwyler, S.; Nelson, B. J. Toward Targeted Retinal Drug Delivery with Wireless Magnetic Microrobots. *Intelligent Robots and Systems*, 2008. *IROS 2008. IEEE/RSJ International Conference on* 2008, pp 1921–1926.
11. Ashkin, A. Forces of a Single-beam Gradient Laser Trap on a Dielectric Sphere in the Ray Optics Regime. *Biophys. J.* **1992**, *61*, 569–582.
12. Grier, D. G. A Revolution in Optical Manipulation. *Nature* **2003**, *424*, 810–816.
13. Svoboda, K.; Block, S. M. Biological Applications of Optical Forces. *Annu. Rev. Biophys. Biomol. Struct.* **1994**, *23*, 247–285.
14. Juan, M. L.; Righini, M.; Quidant, R. Plasmon Nano-optical Tweezers. *Nat. Photonics* **2011**, *5*, 349–356.
15. Pamme, N. Magnetism and Microfluidics. *Lab Chip* **2006**, *6*, 24–38.
16. Gosse, C.; Croquette, V. Magnetic Tweezers: Micromanipulation and Force Measurement at the Molecular Level. *Biophys. J.* **2002**, *82*, 3314–3329.
17. Abbott, J. J.; Peyer, K. E.; Lagomarsino, M. C.; Zhang, L.; Dong, L.; Kaliakatsos, I. K.; Nelson, B. J. How Should Microrobots Swim? *Int. J. Rob. Res.* **2009**, *28*, 1434–1447.
18. Dreyfus, R.; Baudry, J.; Roper, M. L.; Fermigier, M.; Stone, H. A.; Bibette, J. Microscopic Artificial Swimmers. *Nature* **2005**, *437*, 862–865.
19. Zhang, L.; Abbott, J. J.; Dong, L.; Kratochvil, B. E.; Bell, D.; Nelson, B. J. Artificial Bacterial Flagella: Fabrication and Magnetic Control. *Appl. Phys. Lett.* **2009**, *94*, 064107–3.
20. Zhang, L.; Abbott, J. J.; Dong, L.; Peyer, K. E.; Kratochvil, B. E.; Zhang, H.; Bergeles, C.; Nelson, B. J. Characterizing the Swimming Properties of Artificial Bacterial Flagella. *Nano Lett.* **2009**, *9*, 3663–3667.
21. Ghosh, A.; Fischer, P. Controlled Propulsion of Artificial Magnetic Nanostructured Propellers. *Nano Lett.* **2009**, *9*, 2243–2245.
22. Tierno, P.; Golestanian, R.; Pagonabarraga, I.; Sagués, F. Magnetically Actuated Colloidal Microswimmers. *J. Phys. Chem. B* **2008**, *112*, 16525–16528.
23. Tierno, P.; Golestanian, R.; Pagonabarraga, I.; Sagués, F. Controlled Swimming in Confined Fluids of Magnetically Actuated Colloidal Rotors. *Phys. Rev. Lett.* **2008**, *101*, 218304.
24. Lauga, E.; Powers, T. R. The Hydrodynamics of Swimming Microorganisms. *Rep. Prog. Phys.* **2009**, *72*, 096601.
25. Berg, H. C. *E. coli in Motion.*; AIP Press/Springer-Verlag: New York, 2004.
26. Zhang, L.; Petit, T.; Lu, Y.; Kratochvil, B. E.; Peyer, K. E.; Pei, R.; Lou, J.; Nelson, B. J. Controlled Propulsion and Cargo Transport of Rotating Nickel Nanowires near a Patterned Solid Surface. *ACS Nano* **2010**, *4*, 6228–6234.
27. Tottori, S.; Zhang, L.; Qiu, F.; Krawczyk, K. K.; Franco-Obregón, A.; Nelson, B. J. Magnetic Helical Micromachines: Fabrication, Controlled Swimming, and Cargo Transport. *Adv. Mater.* **2012**, *24*, 811–816.

28. Schamel, D.; Mark, A. G.; Gibbs, J. G.; Miksch, C.; Morozov, K. I.; Leshansky, A. M.; Fischer, P. Nanopropellers and Their Actuation in Complex Viscoelastic Media. *ACS Nano* **2014**, *8*, 8794–8801.
29. Nelson, B. J.; Peyer, K. E. Micro-and Nanorobots Swimming in Heterogeneous Liquids. *ACS Nano* **2014**, *8*, 8718–8724.
30. Gao, W.; Feng, X.; Pei, A.; Kane, C. R.; Tam, R.; Hennessy, C.; Wang, J. Bioinspired Helical Microswimmers Based on Vascular Plants. *Nano Lett.* **2014**, *14*, 305–310.
31. Cheng, R.; Huang, W.; Huang, L.; Yang, B.; Mao, L.; Jin, K.; ZhuGe, Q.; Zhao, Y. Acceleration of Tissue Plasminogen Activator-Mediated Thrombolysis by Magnetically Powered Nanomotors. *ACS Nano* **2014**, *8*, 7746–7754.
32. Venugopalan, P. L.; Sai, R.; Chandorkar, Y.; Basu, B.; Shivashankar, S.; Ghosh, A. Conformal Cytocompatible Ferrite Coatings Facilitate the Realization of a Nanovoyager in Human Blood. *Nano Lett.* **2014**, *14*, 1968–1975.
33. Tottori, S.; Sugita, N.; Kometani, R.; Ishihara, S.; Mitsuishi, M. Selective Control Method for Multiple Magnetic Helical Microrobots. *J. Micro-Nanomechatronics* **2011**, *6*, 89–95.
34. Mahoney, A. W.; Nelson, N. D.; Peyer, K. E.; Nelson, B. J.; Abbott, J. J. Behavior of Rotating Magnetic Microrobots above the Step-out Frequency with Application to Control of Multi-Microrobot Systems. *Appl. Phys. Lett.* **2014**, *104*, 144101.
35. Ramaswamy, S. The Mechanics and Statistics of Active Matter. *Mech. Stat. Act. Matter* **2010**, *1*, 323–345.
36. ten Hagen, B.; Kümmel, F.; Wittkowski, R.; Takagi, D.; Löwen, H.; Bechinger, C. Gravitaxis of Asymmetric Self-propelled Colloidal Particles. *Nat. Commun.* **2014**, *5*, No. 4829.
37. Hawkeye, M. M.; Brett, M. J. Glancing Angle Deposition: Fabrication, Properties, and Applications of Micro- and Nanostructured Thin Films. *JJ. Vac. Sci. Technol., A* **2007**, *25*, 1317–1335.
38. Ghosh, A.; Mandal, P.; Karmakar, S.; Ghosh, A. Analytical Theory and Stability Analysis of an Elongated Nanoscale Object under External Torque. *Phys. Chem. Chem. Phys.* **2013**, *15*, 10817–10823.
39. Ghosh, A.; Paria, D.; Singh, H. J.; Venugopalan, P. L.; Ghosh, A. Dynamical Configurations and Bistability of Helical Nanostructures under External Torque. *Phys. Rev. E* **2012**, *86*, 031401.
40. Ghosh, A.; Paria, D.; Rangarajan, G.; Ghosh, A. Velocity Fluctuations in Helical Propulsion: How Small Can a Propeller Be. *J. Phys. Chem. Lett.* **2013**, *5*, 62–68.
41. Lauga, E. Life Around the Scallop Theorem. *Soft Matter* **2011**, *7*, 3060–3065.
42. Purcell, E. M. Life at Low Reynolds Number. *Am. J. Phys.* **1977**, *45*, 3–11.
43. Wagner, G. L.; Lauga, E. Crawling Scallop: Friction-based Locomotion with One Degree of Freedom. *J. Theor. Biol.* **2013**, *324*, 42–51.
44. Mandal, P.; Ghosh, A. Observation of Enhanced Diffusivity in Magnetically Powered Reciprocal Swimmers. *Phys. Rev. Lett.* **2013**, *111*, 248101.
45. Peyer, K. E., Zhang, L., Kratochvil, B., and Nelson, B. J. In Non-ideal Swimming of Artificial Bacterial Flagella near a Surface, In *Proceedings of ICRA*; IEEE: 2010; pp 96−101.
46. Diller, E.; Miyashita, S.; Sitti, M. Remotely Addressable Magnetic Composite Micropumps. *RSC Adv.* **2012**, *2*, 3850–3856.
47. Diller, E.; Giltinan, J.; Sitti, M. Independent Control of Multiple Magnetic Microrobots in Three Dimensions. *Int. J. Rob. Res.* **2013**, *32*, 614–631.
48. Martel, S.; Mohammadi, M.; Felfoul, O.; Zhao, L.; Pouponneau, P. Flagellated Magnetotactic Bacteria as Controlled MRI-trackable Propulsion and Steering Systems for Medical Nanorobots Operating in the Human Microvasculature. *Int. J. Rob. Res.* **2009**, *28*, 571–582.
49. Martel, S.; Tremblay, C. C.; Ngakeng, S.; Langlois, G. Controlled Manipulation and Actuation of Micro-objects with Magnetotactic Bacteria. *Appl. Phys. Lett.* **2006**, *89*, 233904–3.
50. Fournier-Bidoz, S.; Arsenault, A. C.; Manners, I.; Ozin, G. A. Synthetic Self-propelled Nanorotors. *Chem. Commun.* **2005**, 441–443.
51. Baraban, L.; Makarov, D.; Streubel, R.; Mönch, I.; Grimm, D.; Sanchez, S.; Schmidt, O. G. Catalytic Janus Motors on Microfluidic Chip: Deterministic Motion for Targeted Cargo Delivery. *ACS Nano* **2012**, *6*, 3383–3389.
52. Paxton, W. F.; Kistler, K. C.; Olmeda, C. C.; Sen, A.; St. Angelo, S. K.; Cao, Y.; Mallouk, T. E.; Lammert, P. E.; Crespi, V. H. Catalytic Nanomotors: Autonomous Movement of Striped Nanorods. *J. Am. Chem. Soc.* **2004**, *126*, 13424–13431.
53. Hong, Y.; Velegol, D.; Chaturvedi, N.; Sen, A. Biomimetic Behavior of Synthetic Particles: From Microscopic Randomness to Macroscopic Control. *Phys. Chem. Chem. Phys.* **2010**, *12*, 1423–1435.
54. Paxton, W. F.; Sundararajan, S.; Mallouk, T. E.; Sen, A. Chemical Locomotion. *Angew. Chem., Int. Ed.* **2006**, *45*, 5420–5429.
55. Patra, D.; Sengupta, S.; Duan, W.; Zhang, H.; Pavlick, R.; Sen, A. Intelligent, Self-powered, Drug Delivery Systems. *Nanoscale* **2013**, *5*, 1273–1283.
56. Venugopalan, P. L.; Gupta, G.; Ghosh, A.; Singh, H. J.; Nair, G.; Ghosh, A. Study of the Formation of Nano-Networks in Colloidal Particles. *Int. J. Polym. Mater. Polym. Biomater.* **2013**, *62*, 499–501.